Eur. Phys. J. C (2008) 56: 557–569
DOI 10.1140/epjc/s10052-008-0676-5

THE EUROPEAN PHYSICAL JOURNAL C

Regular Article - Theoretical Physics

From Euclidean to Minkowski space with the Cauchy–Riemann equations

Mercedes Gimeno-Segovia, Felipe J. Llanes-Estrada[a]

Departamento de Física Teórica I, Universidad Complutense, 28040 Madrid, Spain

Received: 27 May 2008 / Revised: 25 June 2008 / Published online: 5 August 2008

Abstract We present an elementary method to obtain Green's functions in non-perturbative quantum field theory in Minkowski space from Green's functions calculated in Euclidean space. Since in non-perturbative field theory the analytical structure of amplitudes often is unknown, especially in the presence of confined fields, dispersive representations suffer from systematic uncertainties. Therefore, we suggest to use the Cauchy–Riemann equations, which perform the analytical continuation without assuming global information on the function in the entire complex plane, but only in the region through which the equations are solved. We use as example the quark propagator in Landau gauge quantum chromodynamics, which is known from lattice and Dyson–Schwinger studies in Euclidean space. The drawback of the method is the instability of the Cauchy–Riemann equations against high-frequency noise,which makes it difficult to achieve good accuracy. We also point out a few curious details related to the Wick rotation.

PACS 11.10.St · 11.55.Bq

1 The Wick rotation

Central to non-perturbative quantum field theory is the computation of Green's functions, the vacuum expectation value of quantum operators. These and the related scattering matrix elements are most often computed in Euclidean space, defined by the transformation

$$t \to -\mathrm{i}t_{\mathrm{E}}, \qquad k_0 \to \mathrm{i}k_0. \tag{1}$$

This coordinate transformation is known as "Wick rotation" (see for example [1] for a short account). There are many advantages in solving the field equations in terms of the rotated variables to obtain the so-called Schwinger functions, and we list some in Sect. 2.

[a] e-mail: fllanes@fis.ucm.es

Once the wanted functions have been computed in Euclidean (momentum) space $k_{\mathrm{E}} = (\mathrm{i}k_0, \mathbf{k})$ one would wish to recover the original Minkowski space Green's functions by inverting the Wick rotation. This is possible in perturbation theory at low orders [2, 3] where one has explicit expressions for the functions, and their analytical structure (poles, cuts, essential singularities) is at hand, so that one can employ Cauchy's theorem and collect dispersive cut integrals or pole residues, if need be, and obtain the Minkowski space Green's function by analytical continuation.

For example, to obtain the electron propagator in momentum space (Fourier transform of the probability amplitude for the electron to reach point x if it was originally at the origin 0),

$$S(p) = \int \mathrm{d}^4x\, \mathrm{e}^{-\mathrm{i}x\cdot p} S(x,0) = \mathrm{i}Z\big(p^2\big)\frac{\not{p} + M(p^2)}{p^2 - M^2(p^2) + \mathrm{i}\epsilon}, \tag{2}$$

one would perform the Wick rotation $p_0 \to \mathrm{i}p_{0\mathrm{E}}$ and obtain a function $S(p_{\mathrm{E}})$ as a perturbation of its free-field values ($M(p^2) = m$, $Z(p^2) = 1$). With the function explicitly known, one just extends it into the complex plane and simply substitutes its argument $p_{0\mathrm{E}}$ by $-\mathrm{i}p_0$. If the function is not fully known but its analytical structure is, one employs Cauchy's theorem, as mentioned.

However, in non-perturbative quantum field theory one is seldom in this desirable situation. More often than not, the function has been calculated with the help of a computer, be it by solving the Dyson–Schwinger equation [4] with some carefully designed truncation, or by trying a Monte Carlo evaluation averaging over a small number of configurations on a lattice [5].

The outcome is that the function is then known for Euclidean momenta, typically $k_{\mathrm{E}}^2 > 0$, and an extension into the complex plane becomes necessary to reach the negative axis $k_{\mathrm{E}}^2 < 0$ and $k_{\mathrm{E}}^2 = -k^2$. For non-perturbative functions

one sometimes ignores the precise analytic structure in the complex plane. This situation is worsened in theories where the field quanta do not appear in asymptotic states, except in very specific combinations, such as is presumably the case for quantum chromodynamics.

Attempts have of course been made to solve the problem. An obvious approach is to perform a theory-motivated fit to the computer data, using built-in well educated guesses on what the analytical structure of the continued function must be [6, 7].

Another possibility is to write a spectral representation in terms of a Stieltjes transform yielding a spectral density ρ,

$$S(p^2) = \int \mathrm{d}p \, \frac{\rho(m^2)}{p^2 - m^2 + \mathrm{i}\epsilon} \tag{3}$$

(we have eliminated the spin structure) and then solving the Dyson–Schwinger equation directly "in Minkowski space" for ρ, finally inverting the Stieltjes transform to recover the propagator or Bethe–Salpeter wanted function [8–11]. It is of course clear that in writing the spectral representation, one is already assuming a given cut structure for the function. It is known that, for local quantum field theories where the quanta appear in the final state, the propagator in coordinate space in the upper-half x complex plane is analytic [3], but for confined quanta many questions remain.

In this paper we enrich the toolbox by putting forward a very simple method that does not require the function's analytical structure to be known on the entire complex plane. We observe that the analyticity of a given function cannot only be formulated globally, through satisfaction of Cauchy's theorem, but also locally, through satisfaction of the Cauchy–Riemann equations. By integrating this simple first order differential system with initial condition the function in a given region computed by other means (DSE, lattice, exact renormalization group equations, etc. [12–15]), one can achieve two goals. First, the numerically obtained solution can break down at a given point or line in the plane, indicating perhaps a pole or other singularity. Second, if the region where the system is integrated avoids such singularities, one can obtain the analytical extension (within errors and non-uniqueness) to another region in the complex plane.

We use as an example the behavior of the quark mass function in Landau gauge QCD, $M(p^2)$, that we analytically continue from positive Euclidean virtuality ($p^2 > 0$) into Minkowski space with ($p^2 < 0$). This is plotted in Fig. 1 It can be seen that, within the statistical errors inherited from the lattice data and the systematic numerical errors intrinsic to our procedure, the mass function decreases with increasing Minkowski p^2. Our result keeps open the possibility of a pole of the quark propagator for real p^2 (whose absence has been at times thought of as a possible sign of confinement).

The rest of the paper consists of four sections. In Sect. 2 we make a few comments, some common place but others quoted less often, about the advantages of initially working in Euclidean space. In Sect. 3 we present the Cauchy–Riemann method with one practical case, the quark propagator. A few theoretical comments about errors involved in the process and the generalization to more dimensions are left for Sect. 4. Our discussion is summarized in Sect. 5.

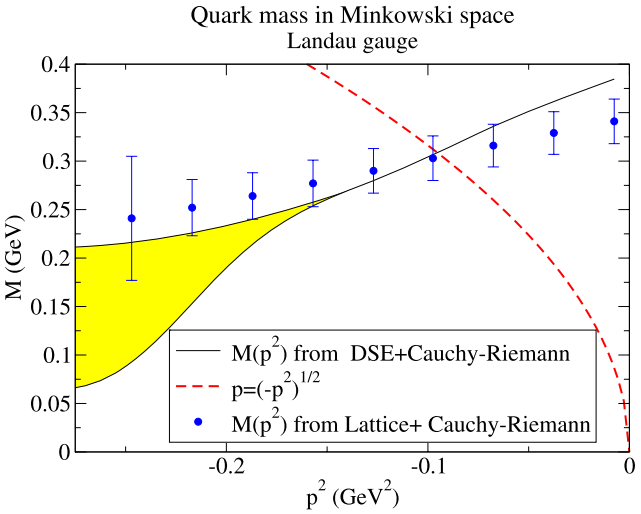

Fig. 1 The analytical continuation to negative Euclidean squared momentum (positive quark virtuality in Minkowski space) of the Landau gauge quark mass function. The yellow band is obtained with input from an Euclidean Dyson–Schwinger calculation, where the Cauchy–Riemann equations have been solved with the θ method in different grids. The Lattice data are likewise analytically continued with the Cauchy–Riemann equations. At low p^2 the error is dominated by the original lattice statistical error, and eventually the build-up of numerical errors in the Cauchy–Riemann equations dominate. The trend of $\mathrm{Re}(M)$ is clearly decreasing with p^2, and therefore a pole in the quark propagator is expected. Since $\mathrm{Im}(M)$, presented later on, is small, this pole is on or close to the real axis, with $M = 305(25)$ MeV. The lattice data that are analytically continued are from Ref. [15]

2 Working in Euclidean space

In lattice formulations of quantum field theory, the field configurations over which the path integral is evaluated are randomly generated according to a distribution $\mathrm{e}^{-\int \mathrm{d}t\, \mathcal{L}}$, which is the Wick rotation of the actual quantum weight for the path integral, $\mathrm{e}^{\mathrm{i}\int \mathrm{d}t\, \mathcal{L}}$. Green's functions computed thereafter on the lattice are valid in Euclidean space. Even if working in Minkowski space, a popular way of "minimally" regularizing in the path integral formalism is to rotate the time integration into the complex plane,

$$\int \mathrm{d}^4x = \lim_{T\to\infty} \int_{-T\times(1-\mathrm{i}\epsilon)}^{T\times(1+\mathrm{i}\epsilon)} \mathrm{d}t \int \mathrm{d}^3x.$$

Beyond the convergence of the path integral and the weighting configurations inside a compact set of function space, there are several more advantages.

One is that the Dyson–Schwinger equations, whose solutions are often used to interpret the lattice data, are extremely difficult to solve on a computer in Minkowski space. Indeed, a typical DSE is that for the mass function of a fermion in the presence of a scalar field, with Yukawa coupling, in the rainbow approximation:

$$M(p) = c \int \mathrm{d}^4 k \frac{M(k)}{(k^2 - M(k)^2 + \mathrm{i}\epsilon)((k-p)^2 - m_\phi^2 + \mathrm{i}\epsilon)}. \tag{4}$$

If one solves the equation iteratively by guessing M_0, one notices that the position of the fermion pole in the denominator is not known after the first iteration, and it needs to be determined numerically (an attempt at carrying on this program exists [16]).

However, it is common use to Wick rotate the k integration variable to Euclidean space. If p is likewise rotated, the resulting equation is easier to program as the denominator poles are on the left k^2 plane, out of the numerical integration region in the radial k^2 variable. We have

$$M(p) = c \int \mathrm{d}^4 k \frac{M(k)}{(k^2 + M(k)^2 + \mathrm{i}\epsilon)((k-p)^2 + m_\phi^2 + \mathrm{i}\epsilon)} \tag{5}$$

(c represents constants irrelevant to the discussion).

Note also that when working in Euclidean space, a discrete subgroup of the Euclidean rotation group is retained. For example, for a simple cubic lattice with ($x = ai_x$, $y = ai_y$, $z = ai_z$, $t = ai_t$), invariance under rotations by $\pi/2$ is explicit. This can be exploited to study the quantum representations of the discrete group, then trying to match the resulting states to a representation of the full continuous group.

However, in Minkowski space there is no finite lattice that retains invariance under a non-trivial subgroup of the Lorentz group. If a grid is invariant under discrete Lorentz transformations of the parameter a, then it has infinitely many points. We discuss Lorentz invariant discretizations of Minkowski space in the appendix.

One further motivation is the non-compactness of the equal k^2 hypersurfaces. While in Euclidean space the condition $k^2 = \Lambda^2$ determines a hypersphere's surface, so that

$$\int^{\Lambda} \mathrm{d}^4 k_\mathrm{E}\, f\left(k_\mathrm{E}^2\right) = 2\pi^2 \int^{\Lambda} k_\mathrm{E}^3\, \mathrm{d}k_\mathrm{E}\, f\left(k_\mathrm{E}^2\right) \tag{6}$$

can be factorized into a radial integral and a finite $2\pi^2$ solid hyperangle (the hyperarea of a unit-radius hypersphere's surface), this is not possible in Minkowski space. In this space, the corresponding unit-hyperboloid $k^2 = 1$ has infinite hypersurface. Therefore, integrals of Lorentz invariant functions are by necessity divergent even after regulation of large virtualities, and they are only defined by analytical continuation from Euclidean space.

In perturbation theory, a much used method is to perform the k_0 integrals first, usually with a pole analysis, and later impose a cutoff on space-like momentum $\mathbf{k}$. However, this cutoff is frame-dependent, and there is no direct method that manifestly preserves Lorentz invariance.

From all these arguments, it is hard to conceive progress in non-perturbative quantum field theory in Minkowski space without progress in complex-plane analytical continuation for the relevant functions. This paper is a modest contribution in this direction, with the interest in keeping the discussion alive.

3 Numerical solution of the Cauchy–Riemann equations

3.1 Cauchy–Riemann equations in polar coordinates

If u and v are respectively the real and imaginary parts of a complex function of one complex variable $p^2 = r\mathrm{e}^{\mathrm{i}\theta}$, the Cauchy–Riemann equations in polar coordinates read

$$\frac{\partial v}{\partial \theta} = r \frac{\partial u}{\partial r}, \tag{7}$$

$$\frac{\partial u}{\partial \theta} = -r \frac{\partial v}{\partial \theta}. \tag{8}$$

Given the initial conditions $u(r,0) = u_0(r)$ and $v(r,0) = v_0(r)$ on a segment of the real p^2 axis, corresponding to $\theta = 0$, one can then evolve the system towards increasing and decreasing θ (like the opening of a fan). For very smooth data sets one can typically reach 90–120 degrees on each side of the fan before the instabilities wipe the solution to infinity. The (Cauchy–Euler) explicit discretization with centered r-derivative on a grid (r_j, θ_i) is simply

$$v(r_j, \theta_{i+1}) = v(r_j, \theta_i) + r_j(\theta_{i+1} - \theta_i) \frac{u(r_{j+1}, \theta_i) - u(r_{j-1}, \theta_i)}{r_{j+1} - r_{j-1}}, \tag{9}$$

$$u(r_j, \theta_{i+1}) = u(r_j, \theta_i) - r_j(\theta_{i+1} - \theta_i) \frac{v(r_{j+1}, \theta_i) - v(r_{j-1}, \theta_i)}{r_{j+1} - r_{j-1}}, \tag{10}$$

where, to solve over an arch taken anticlockwise, $(\theta_{i+1} - \theta_i) > 0$. At the end-points of the grid one cannot use centered derivative, so left (right derivative) is necessary, $(v(r_2, \theta_i) - v(r_1, \theta_i))/(r_2 - r_1)$, etc. The situation is represented in Fig. 2.

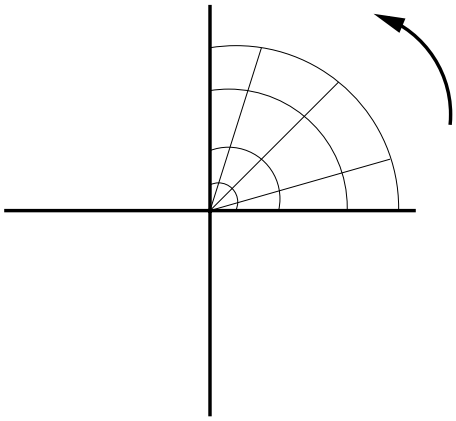

Fig. 2 The Cauchy–Riemann equations in polar coordinates allow us to explore a fan-shaped region of the complex plane where a function is analytic

The use of this method is to provide a cross-check of solutions of the Dyson–Schwinger equations in the complex plane. These are needed to solve the Bethe–Salpeter equations for mesons, since the (external) meson momentum is of course in Minkowski space (real), and the internal quark momentum is Wick rotated to Euclidean space (imaginary), so that one ends solving the DSE inside a parabola in the complex plane symmetric with respect to the real momentum axis. The Cauchy–Riemann equations are currently no match in precision to directly solving the DSE in the complex plane where this is feasible, but they can provide a cross-check that is very simple to programme (compare the trivial linear system above with the complex, non-linear, bidimensional DSE when the angular kernel or vertex are non-trivial).

The Cauchy–Riemann equations, however, are a statement of analyticity, and the solution is a numerical representation of the closest analytical function that contains the initial data. This means that if the "true" function has a pole or a cut, the Cauchy–Riemann iteration will fail to see it and simply separate from that function, and it is likely to diverge soon from accruing instabilities. This is illustrated in Fig. 3.

3.2 Cauchy–Riemann equations on a strip

The advantage of a local formulation of analyticity employing the Cauchy–Riemann equations is lost if one needs to sweep the entire complex plane. Therefore, it is profitable to solve them in Cartesian coordinates, first away from the x axis along y,

$$\frac{\partial u}{\partial y} = -\frac{\partial v}{\partial x}, \tag{11}$$

$$\frac{\partial v}{\partial y} = \frac{\partial u}{\partial x}, \tag{12}$$

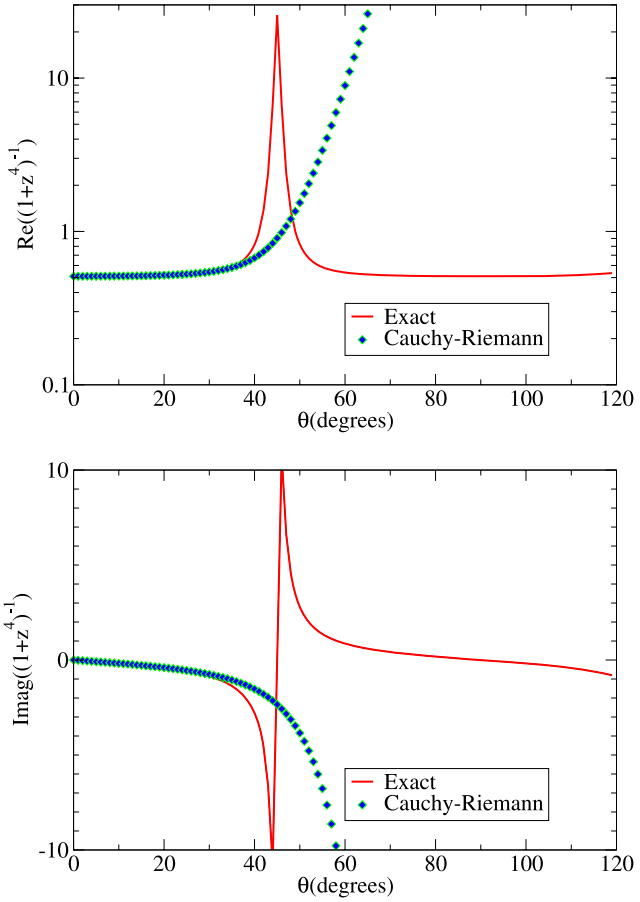

Fig. 3 Real and imaginary part of the function $\frac{1}{1+z^4}$ for $z = re^{i\theta}$ with fixed $r = 0.99$ and varying θ. The dashed line is the computer solution of the Cauchy–Riemann equations in degree steps, with the initial condition given on the positive real half-axis. The function has a pole at $(1+i)/\sqrt{2}$ that the Cauchy–Riemann equations cannot isolate since they entail analyticity. They, however, diverge due to accruing instability in the region where the function has a larger derivative

and then leftwards along x. The method fails if the complex plane is completely cut from $-\infty$ to ∞ along the y axis. In any other situation (the standard half-plane cut of a power-law or logarithm, or a finite number of poles or essential singularities), one can find a path between the right and the left x axis and solve the Cauchy–Riemann equations along them.

We now improve upon the discretization of the differential equations and employ an implicit θ method. This is convenient, since the Cauchy–Riemann equations are quite unstable (as pointed out below in Sect. 4.2). The $\partial_y u$ equation for a point not on the edge of the grid becomes (with the superindex labeling y, the subindex x)

$$\frac{u_i^{j+1} - u_i^j}{y_{j+1} - y_j} = \frac{-1}{x_{i+1} - x_{i-1}} \times \left(\theta\left(v_{i+1}^{j+1} - v_{i-1}^{j+1}\right) + (1-\theta)\left(v_{i+1}^{j} - v_{i-1}^{j}\right)\right). \tag{13}$$

In the advance along y one groups the u_i and v_i for fixed y_j in a vector $\mathbf{u}^j = (u_1^j, v_1^j, u_2^j, v_2^j, \ldots, u_N^j, v_N^j)$ and the θ method's discretization can be written down as a linear problem

$$\mathbf{A}\mathbf{u}^{j+1} = \mathbf{B}\mathbf{u}^j. \tag{14}$$

In the simplest case of equal x subintervals, one can define $r = \theta\Delta y/(2\Delta x)$, then the matrix $\mathbf{A}$ becomes

$$\begin{pmatrix} 1 & -2r & 0 & 2r & 0 & \ldots & & & & \\ 2r & 1 & -2r & 0 & \ldots & & & & & \\ 0 & -r & 1 & 0 & 0 & r & \ldots & & & \\ r & 0 & 0 & 1 & -r & 0 & \ldots & & & \\ \ldots & & & & & & & & & \\ & & & & & \ldots & 0 & -2r & 1 & 2r \\ & & & & \ldots & 0 & 2r & 0 & -2r & 1 \end{pmatrix}, \tag{15}$$

where the third and fourth line are the repeated unit, except that the non-vanishing elements are shifted to the right (the 1 always mark the diagonal, and the matrix is band-diagonal). The matrix $\mathbf{B}$ can likewise be filled by exchanging $\theta \to (1-\theta)$ and changing the sign of all off-diagonal matrix elements of $\mathbf{A}$ (the diagonal of $\mathbf{B}$ likewise contains 1).

The advance in y proceeds by solving the linear system to obtain (u, v) at y_{j+1} from their values at y_j. We use a standard LU factorization, although since the matrix $\mathbf{A}$ is band-diagonal, Crout's algorithm can speed things somewhat. For one complex variable and the small number of points we use, this is irrelevant in computer time.

However, since the advance to the left will have as initial condition the edge (along the y axis) of the first computed block, and in the end we will be interested in the values of the function on the x axis, that is, the edge of the second computed block, it pays off to improve the computation of the derivative at the edge of the block.

The left derivative we have displayed explicitly,

$$\frac{\partial u(x=0,y)}{\partial x} = \frac{u_2^j - u_1^j}{x_2 - x_1} + \mathrm{o}(h) \tag{16}$$

can be interpreted as a centered derivative at the mid-point $(x_2 + x_1)/2$. Considering also the centered derivative at x_2 and extrapolating linearly to x_1, one obtains an improved

$$\frac{\partial u(x=0,y)}{\partial x} = 2\frac{u_2^j - u_1^j}{x_2 - x_1} - \frac{u_3^j - u_1^j}{x_3 - x_1} + \mathrm{o}\big(h^2\big), \tag{17}$$

and likewise at the last N point of the grid, and this slightly complicates the first two and last two rows of $\mathbf{A}$.

Once the advance upwards in the y direction has reached N, one starts an advance to the left as in Fig. 4, and similar considerations apply.

The θ parameter that advances or delays the derivative perpendicular to the integration direction is empirically fixed for now. Several problems are somewhat independent of θ, others have a broad minimum of instability around -1. We find that $\theta = -0.5$ is as good as any. A brief eigenvalue analysis is presented below that explains why, in Sect. 4.2.

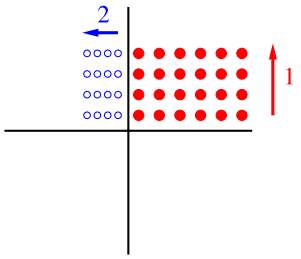

Fig. 4 The Cauchy–Riemann equations in Cartesian coordinates can be used to explore a strip, first upwards along the y axis, then leftwards along the x axis. In this use one only needs analyticity of the function on a strip above (or below) the axis to obtain information on the Minkowski side. The method fails only if the complex plane is completely cut from $-\infty$ to ∞ along the y axis

To show a test of the method, we employ the simple function

$$f_{\mathrm{test}}(z) = \frac{1}{1 + z^2/4}, \tag{18}$$

which has two poles above and below the x axis at $\pm 2\mathrm{i}$. Because of the fast build-up of numerical errors, we need $\Delta y < \Delta x$, so the strip is always shorter in the direction of the advance of the integration (for an $N \times N$ problem). In Figs. 5 and 6, we show the real and imaginary parts calculated with the Cauchy–Riemann equations with the initial condition on the positive real half-axis, plotted along the imaginary and the negative real axis, respectively. Similarly for the function $\cos(z)$ in Figs. 7 and 8.

The method starts to break down for x near zero and $y > 1$, as the pole is approached. But one can see how the part of the strip that goes well below the pole passes cleanly and allows to one reproduce the function on the left axis, given as initial condition the N exact values on the right axis. All in all, the method provides a reasonable representation of the function from the solution of the Cauchy–Riemann equations. Note that the imaginary part, exactly zero on the left axis, is calculated to be of order 1% with a forty-point grid. This should be considered the error of the method, and it is far less than the statistical errors in the lattice data that we will shortly employ.

Should the analytic structure of the function become available, one could devise an appropriate path in the complex plane from the region where the function is known to the region where it is wanted by analytical continuation. The initial value problem can then be formulated with the advance direction along the tangent vector to the path, τ. This vector changes orientation in principle, so one would need to use the "Cartesian-like" formulation to advance and the

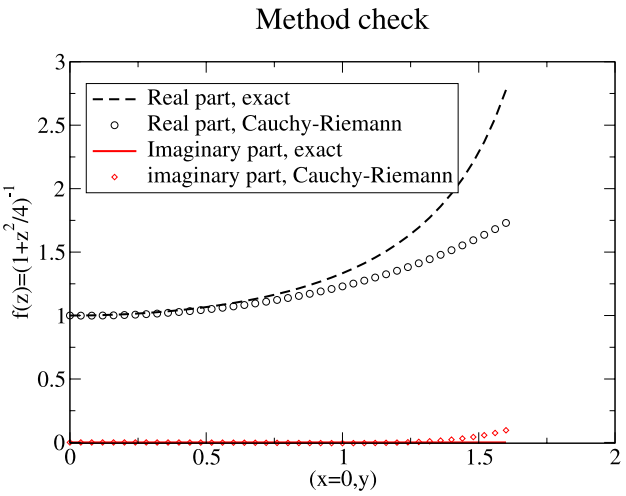

Fig. 5 The function $f_{\text{test}}(z) = \frac{1}{1+z^2/4}$ analytically continued from $(x > 0, y = 0)$ to $(x = 0, y > 0)$, with the Cauchy–Riemann equations. The imaginary part is exactly zero on this imaginary axis, and the function has a pole at $y = 2$

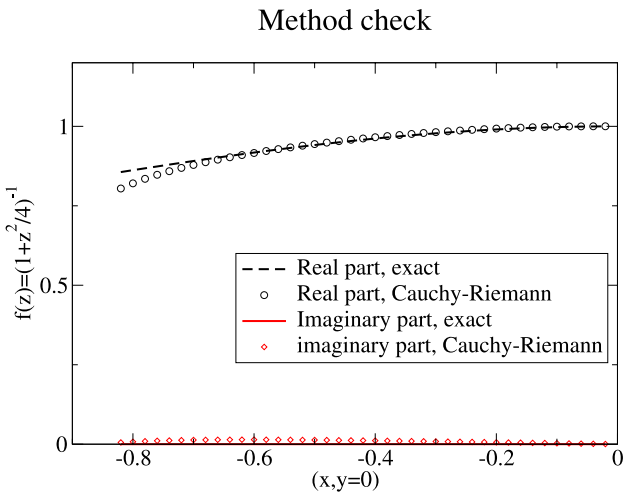

Fig. 6 The function $f_{\text{test}}(z) = \frac{1}{1+z^2/4}$ analytically continued from $(x > 0, y = 0)$ to $(x < 0, y = 0)$, with the Cauchy–Riemann equations

"polar-like" formulation to rotate the direction of advance, in alternate steps.

3.3 Wick rotation of the quark mass function

In the introduction we have advanced, in Fig. 1, our main application, the analytical continuation of the quark mass function $M(p^2)$ in Landau gauge, which we now carefully analyze and justify.

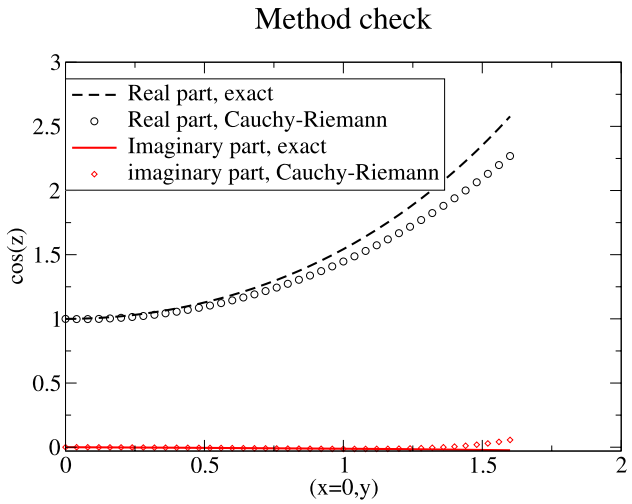

Fig. 7 As in Fig. 5, but for the function $\cos z$

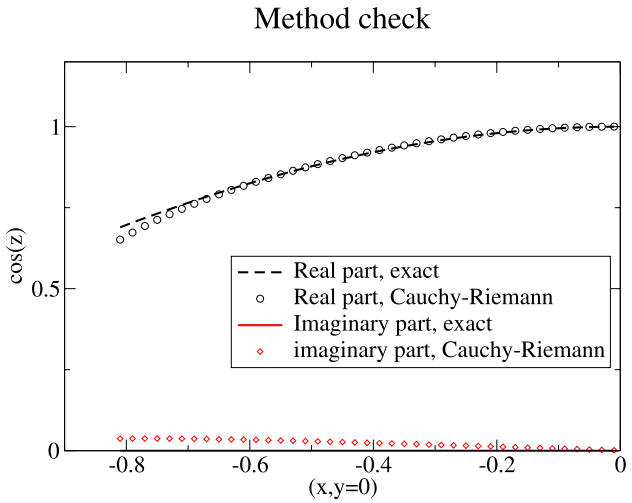

Fig. 8 As in Fig. 6, but for the function $\cos z$

Because of Lorentz invariance applied to a spin 1/2 fermion, the quark propagator can be written in full generality as

$$S(p) = \frac{\mathrm{i}Z(p^2)\not{p}}{p^2 - M^2(p^2)} + \frac{\mathrm{i}Z(p^2)M(p^2)}{p^2 - M^2(p^2)}. \tag{19}$$

As already discussed, the pole in the denominator is a nuisance, usually disposed of by performing the Wick rotation $p_0 \to \mathrm{i}p_{\mathrm{E}}^0$. Concentrating on the denominator, we have

$$\frac{1}{p_0^2 - \mathbf{p}^2 - M^2(p_0^2 - \mathbf{p}^2)} \to \frac{-1}{p_0^2 + \mathbf{p}^2 + M^2(-p_0^2 - \mathbf{p}^2)};$$

the pole is absent for real M. One usually eschews a sign, the function $M^2(-p_0^2 - \mathbf{p}^2)$ is customarily called $M(p_{\mathrm{E}}^2)$, where $p_{\mathrm{E}}^2 > 0$, and we will keep this notation. Hence, to retrieve the mass function that actually appears in the Minkowski

space propagator for positive virtuality p^2, we need to identify it with the analytical continuation of the lattice (or DSE) $M(p_{\mathrm{E}}^2)$ to negative p^2. Note that although the analytical continuation is nominally made in p_0, since $p_0^2 - \mathbf{p}^2$ is a polynomial, it is an analytical function of p_0. We conclude that wherever M is analytical in p_0 it is also analytical in $p_0^2 - \mathbf{p}^2$.

The analytical properties of $M(p^2)$ are not well known, especially for confined quanta such as quarks. However, we note that a pole in this function would imply a zero in the quark propagator, and this, assumed continuous, can be ruled out in the entire region of the complex plane that we sample, from the lattice data on the Euclidean real p^2 axis.

We take the lattice data from [15], see also [17]. This has been provided to us from $28^3 \times 96$ lattices with MILC configurations. We have used $a^{-1} = 2.29$ GeV to set the scale from the internodal spacing.

Due to our sensitivity to large-frequency noise, we only use a subset of the lattice data, taking one of every few points in the interval $p \in (0, 8)$ GeV. The trimming has been performed so that the resulting mass monotonously decreases towards higher momenta (asymptotic freedom), to avoid distortions of analyticity and large errors through a rapidly varying derivative. We further square the abscissa $p \to p^2$, since the latter is the variable in which we perform the analytical continuation. The original lattice data, already in physical GeV units, is given in Fig. 9. We show the actual input set to our code after these manipulations have been performed, faithful to the original data and error bands, but amenable to analytical continuation. The data are renormalized in the MOM scheme, and, as can be seen, the mass at a scale of 8 GeV is 60 MeV with the chosen scale a^{-1}. We further take as input the Dyson–Schwinger calculation from [20]. This input has the advantage that there are no statistical errors and the function is very smooth. In exchange, there are systematic errors (coming from the precise way in which the quark–gluon vertex is treated in that reference), which are unknown and only controllable in the propagator in comparison with lattice data or renormalization group equations. We plot the resulting set in Fig. 10.

Finally, we perform the analytical continuation on a strip in the complex plane above the axis, that presumably avoids non-analyticities in $M(p^2)$ (else a continuation under the axis is possible) and obtain the real part of M advanced in the introduction in Fig. 1.

We also plot in Fig. 11 the imaginary part of the same M function, which, as can be seen, is compatible with zero within the error bands.

From the graphs one can conclude that, just as for the tree-level propagator in perturbation theory, there is a crossing of M and p for (negative Euclidean), positive Minkowski p^2. This means that the actual quark propagator does have a pole at or very near the real axis. It has been quoted [6] to be at (300–500) MeV from the Dyson–Schwinger equations alone. From the analysis of the lattice data set at hand, we conclude that $M(M) = 305(25)$ MeV, in agreement with that estimate. Of course, it would be interesting to compare this with other lattice data sets, and in particular use different current quark masses, so the error band is definitely larger.

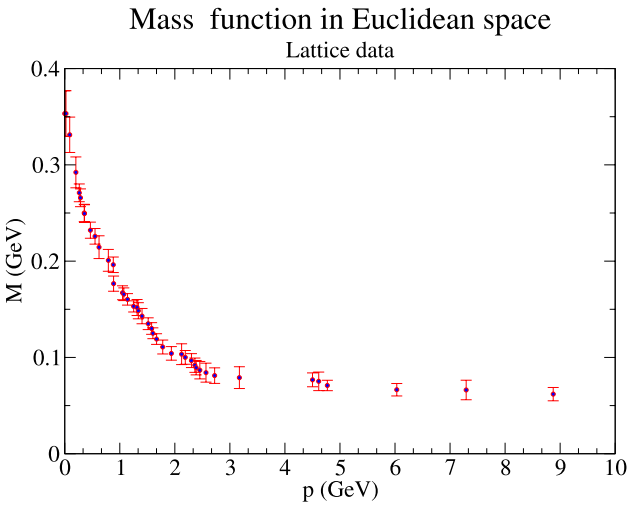

Fig. 9 A part of the lattice data for the quark mass function in Landau gauge QCD. We have trimmed the data to ensure the monotonous decrease in the function and to reduce the high-frequency noise, which grows fast in the Cauchy–Riemann equations. We slightly increased the error bands to cover the omitted points (trading our systematic error in trimming into a statistical error). The lattice data from [15] is normalized to a current quark mass of $m_u = 60$ MeV

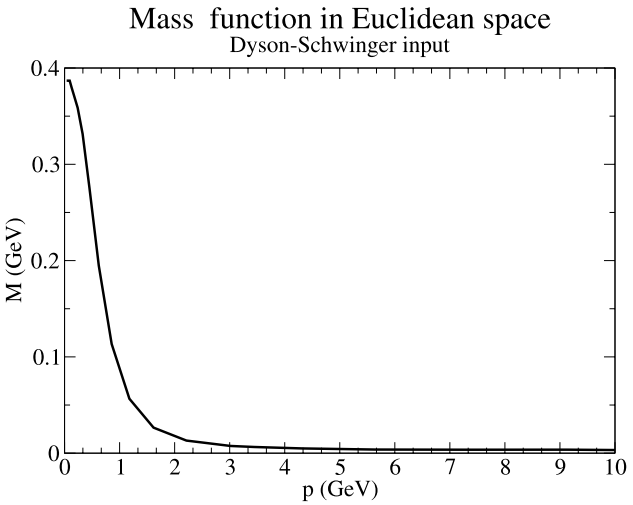

Fig. 10 Input calculation from the Dyson–Schwinger formalism. The current quark mass is 2 MeV at 13 GeV. The function is smoother than the lattice data, reducing high-frequency noise, but in exchange its systematic errors are more difficult to control. The original function reported in [20] decreases at very small momentum; we have been conservative and avoided this by a small variation of the vertex dressing functions

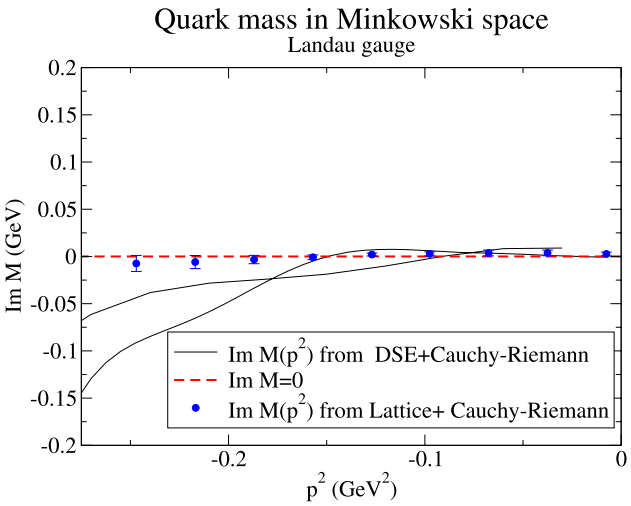

Fig. 11 The Cauchy–Riemann method leads to an imaginary part of the mass function on the left half-axis in Euclidean space that is well compatible with 0. This is in agreement with the outcome of a Taylor expansion around the origin (however, there is no way to tell the convergence radius of such a series, so we deem the Cauchy–Riemann method superior)

We do not find support for the attending conjecture of two conjugate poles with a sizable imaginary part.

4 Some theoretical issues

4.1 Uniqueness

Here we study to what extent the solution of the Cauchy–Riemann equations for the quark mass function is unique, given the initial conditions as the lattice computation on the positive p_{E}^2 half-axis. By standard complex analysis, the uniqueness of an analytic continuation of a function is guaranteed if the function is initially known on an open subset of $\mathbf{C}$.

The positive real half-axis is open in $\mathbf{R}$, but not in $\mathbf{C}$. However, it is easy to show that the analytic continuation is unique. Imagine that u and v are known for $y = 0$ and $x > 0$. Then, all partial derivatives $\frac{\partial^n u}{\partial x^n}$ and $\frac{\partial^n v}{\partial x^n}$ are known. In particular, for the quark mass function, $v(y = 0) = 0$ (and all x-derivatives also vanish), and $u(x, y = 0) = M(x)$, the real mass.

Assume that the extension of M to the complex plane was not unique. Then, in addition to $f = (u, v)$, there would be another function, $f + g$, that would satisfy the Cauchy–Riemann equations with the same initial conditions. Since the sum of two analytic functions is analytic, g itself should be analytic. This means that its components, g_x and g_y, would also satisfy the Cauchy–Riemann equations:

$$\frac{\partial g_x}{\partial y} = -\frac{\partial g_y}{\partial x}, \tag{20}$$

$$\frac{\partial g_y}{\partial y} = \frac{\partial g_x}{\partial x}, \tag{21}$$

with initial condition $g(y = 0) = 0$ exactly, with all derivatives $\frac{\partial^n g(y=0)}{\partial x^n} = 0$ also vanishing on the real axis. Automatically, employing (20), and subsequently deriving it, all y-derivatives also vanish. Therefore, g is exactly zero in the domain of analyticity, and f unique.

Of course, in practice f is only known at a discrete and finite set of points $z_i = (x_y, 0)$, $i = 1, \ldots, N$. An analytic function could oscillate between any two of the points and take arbitrarily large or small values. Therefore, one needs an additional hypothesis to claim that the computed function is a fair representation of the "actual" function.

The sufficient hypothesis is monotony of the function between any two grid points (note that the function might be globally non-monotonous by being allowed to change the derivative sign at the grid points themselves). If the function is strictly decreasing between x_i and x_{i+1}, then the maximum and minimum values that it can take between them are f_i and f_{i+1}, and the function is bound (it being analytic, it is also continuous). Then, to arbitrarily shrink the error in our knowledge of the initial condition, one just needs to arbitrarily shrink the grid spacing, so as to further constrain the function in every subinterval. The function computed with the discretized Cauchy–Riemann equations will be as close to the true function as the stability of the system allows, given the bound error in the initial conditions.

For our example, the light quark propagator, there is essentially no question that the mass function is monotonously decreasing towards larger momenta. This is known at large momentum from asymptotic QCD and at low momentum from all studies of the Dyson–Schwinger equations and lattice studies (where all non-monotonous behavior has way less than 1σ significance and can be safely called noise). The hypothesis of monotony can be checked (falsified) with lattice data by simply decreasing the link size in the grid, while at the same time reducing the statistical error bar.

One more caveat may be raised. Imagine adding to the "actual" function $f(u, v)$ another analytical function $g(u, v)$, such that g is very near zero on the right (Euclidean) axis and very large on the left hand (Minkowski) side. Then, while $f + g$ does not exceed the error bars for f on the initial data, it completely changes the answer on output, since $f + g$ is very different from f on the right half-axis. Of course, the derivative of the function must be very large around $u = 0$, since the function changes from very small to sizable in a small interval. To bind this derivative from above and exclude this unpleasant possibility, one needs to demand an additional condition, since exact knowledge of all derivatives of the function or knowledge of the function in the entire interval is, in a computer grid representation, unavailable.

Now, a fast change of the derivative beyond what is visible from the data points implies that the second derivative is not well represented by its discrete approximation. Here, one may demand monotony of the second derivative of the function between the last three (few) points of the grid on the interval x_1, x_2, x_3. This guarantees that the extrapolation of the derivative at just the last grid point does not grow arbitrarily, since the second derivative remains bound. This is now quite a technical condition, and maybe not optimal, others being possible.

4.2 Instability of large-frequency noise

Let us now consider the effect of a perturbation on the system of Cauchy–Riemann equations (20). Since the system is linear, it accepts a Fourier analysis. Let us perform it on the x variable, so that the Fourier decomposition is

$$g_x(x,y) = A(k,y)\mathrm{e}^{\mathrm{i}kx}, \qquad (22)$$
$$g_y(x,y) = B(k,y)\mathrm{e}^{\mathrm{i}kx}.$$

Then the system of equations becomes

$$\frac{\partial}{\partial y}\begin{pmatrix} A \\ B \end{pmatrix} = \begin{bmatrix} 0 & -\mathrm{i}k \\ \mathrm{i}k & 0 \end{bmatrix}\begin{pmatrix} A \\ B \end{pmatrix}, \qquad (23)$$

and therefore

$$\begin{pmatrix} A \\ B \end{pmatrix} = \begin{bmatrix} \cosh ky & -\mathrm{i}\sinh ky \\ \mathrm{i}\sinh ky & \cosh ky \end{bmatrix}\begin{pmatrix} A_0 \\ B_0 \end{pmatrix} \qquad (24)$$

in terms of the initial condition on the x axis. Obviously, if the exact solution is initially perturbed due to computer inaccuracies by an amount δA_0, with $B_0 = \delta B_0 = 0$ for simplicity, then at large distances the perturbation on the computed solution exponentiates:

$$\delta A, \delta B \propto \mathrm{e}^{ky}|\delta A_0|.$$

This could of course be anticipated by remembering that the solutions of the Cauchy–Riemann equations are two-dimensional harmonic functions, so that the separable solutions are sinusoidal functions times exponentials, $\cos kx \cosh ky$, etc.

This is especially worrisome when using Monte Carlo data for the initial condition, since the local (high-k) noise spoils the stability very soon. Thus, one needs to apply a cooling algorithm or trim the data first to remove short-distance fluctuations, justifying our keeping only part of the lattice data to ensure monotony. Large-distance, systematic shifts of the initial condition are less perturbing. In Fig. 12 we capture the u (real part) noisiest eigenvector of the iteration matrix $\mathbf{A}^{-1}\mathbf{B}$ for a particular $\theta = -0.5$ method for fixed grid size, to show its increasing wavenumber.

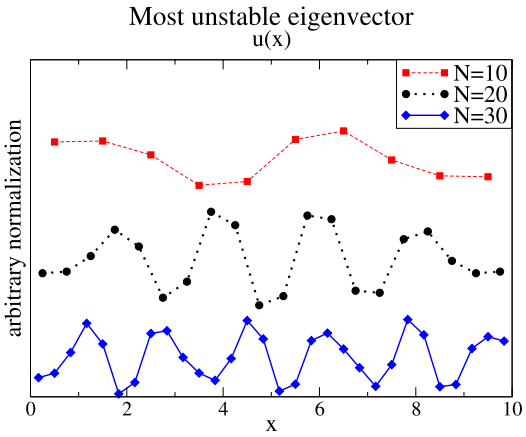

Fig. 12 The most unstable eigenvector as a function of the number of points transverse to the direction of advance, for the iteration matrix in the Cauchy–Riemann $\theta = -0.5$ discretization. The functions have been vertically shifted for visibility

Table 1 Largest eigenvalue (one of a pair) for the iteration matrix of the θ method

θ	$\frac{\Delta y}{\Delta x}$	$\lvert\lambda\rvert$
2.5	1	9.8
2.0	1	2.6
1.5	1	11
1.0	1	13
0.5	1	2.7
0.1	1	2.0
−0.1	1	1.8
−0.5	1	1.6
−1.0	1	11
−1.5	1	13
−2.0	1	2.7
−2.5	1	7.8
−0.5	$\frac{1}{2}$	1.4
−0.5	$\frac{1}{4}$	1.2
−0.5	$\frac{1}{6}$	1.14
−0.5	$\frac{1}{8}$	1.11
−0.5	$\frac{1}{10}$	1.08

The iteration matrix $\mathbf{A}^{-1}\mathbf{B}$ always has eigenvectors that are larger than 1 in modulus. We have studied them for very simple equispaced rectangular grids, with the direction of advance along y. For a fixed ratio of the increments, $\frac{\Delta y}{\Delta x}$, the largest eigenvalue is quite independent of the number of grid points (this is obvious from the definition of the matrix). The dependence on θ and $\frac{\Delta y}{\Delta x}$ can be followed from Table 1.

Note from the table that, unlike for the heat equation, the θ method is not convergent. We are not able to approach a given function with arbitrary accuracy, but only

provide an estimate. It is apparent that decreasing the advance step $\frac{\Delta y}{\Delta x}$ is not a winning strategy, since, for example, fixing $\theta = -0.5$, with $\frac{\Delta y}{\Delta x} = 1$, $|\lambda| = 1.6$, and to advance the same distance with $\frac{\Delta y}{\Delta x} = 1/10$, one needs ten steps, but $1.08^{10} = 2.1 > 1.6$, meaning that with a smaller step, one can advance less far in the progress direction, since errors amplify faster. (Of course, by decreasing the step, one does obtain a more reliable representation of the function for short advance distances.)

4.3 Generalization to several complex variables

In principle, it would appear straightforward to generalize the Wick rotation to several dimensions. For example, let us consider a vertex function in field theory, say the quark and gluon or the electron–photon three-point functions. These are characterized by twelve Dirac tensors multiplied by the amplitudes of the three independent Lorentz scalar variables, the squared momenta of each of the particles,

$$\lambda_i\big(p_1^2, p_2^2, q^2\big), \quad i = 1, \ldots, 12.$$

Given the lattice data in Euclidean space,

$$\lambda_i\big(p_{1\mathrm{E}}^2, p_{2\mathrm{E}}^2, q_{\mathrm{E}}^2\big), \quad i = 1, \ldots, 12,$$

one would need to perform the inverse Wick rotation to negative p_E^2 in each of the variables, in practice solving the Cauchy–Riemann equations variable by variable. Notice that if the power-law solutions of [20] are correct, then one expects a cut at zero virtuality, $q^2 = 0$, in the gluon variable, but this can be avoided by appropriately deforming the region where one solves the Cauchy–Riemann equation.

Now let us examine a curious detail that does not come about in one dimension. If there is only one variable, $p^2 = 0$ defines the light-cone in Minkowski space, a three-dimensional manifold in four-dimensional space. However, $p_{\mathrm{E}}^2 = 0$ defines the origin in Euclidean space, this being just a point (this is just another manifestation of the difference between the compact rotation group and the unbound Lorentz group). The interesting observation is that, upon Wick rotation, $f(p_{\mathrm{E}}^2 = 0)$, the value of a Green's function at one point in Euclidean space, becomes $f(p^2 = 0)$, the value of the same Green's function on the entire light-cone.

But what happens in more dimensions? One may know the value of the function $\lambda(p_{\mathrm{E}1}^2 = 0, p_{\mathrm{E}2}^2, p_{\mathrm{E}2}^2)$ in Euclidean space at the origin for the variable $p_{\mathrm{E}1}$. But in Minkowski space, $p_1^2 = 0$ does not imply $p_1 = 0$; hence the function takes different values for different points of the p_1 light-cone, $\lambda(p_1^2 = 0, p_2^2, (p_1 - p_2)^2)$, which do not coincide with the value at the origin in Euclidean space.

This comes about because in a three-point function there are two reference four-vectors, p_1 and p_2, and while the Euclidean point with $p_1 = 0$ is at a fixed distance from the $p_2 = 0$ point, its Minkowski image is not.

4.4 Taylor expansion

Analytical functions accept Taylor expansions of the type

$$f(z) = \sum_{n=0}^{\infty} \frac{(z - z_0)^n}{n!} f^{(n)}(z_0). \tag{25}$$

One could think of performing a polynomial fit to a given set of data points $(z_i, f(z_i))$ to represent the function within the radius of convergence of the series. One would simply need to solve the Vandermonde system for N points,

$$f(z_i) = \sum_{n=0}^{N} (z - z_0)^N \left(\frac{f^{(n)}(z_0)}{n!} \right). \tag{26}$$

For example, expanding around the origin, the matrix of coefficients for the linear system is the Vandermonde matrix with rows $(1, z_i, z_I^2, \ldots, z_i^N)$. Once the system has been solved for the derivatives $(\frac{f^{(n)}(z_0)}{n!})$, they can be substituted in (25) to obtain the function at an arbitrary point.

One could argue that this is the simplest local implementation of analyticity, and one may wonder why one should worry about the Cauchy–Riemann equations at all. Of course, in practice monotony is difficult to achieve with a finite number of polynomials: the approximant will oscillate between the tabulated grid points with the lattice data. In addition, should there be a cut starting at $p^2 = 0$ in the complex plane, that would not be surprising in view of the power-law representations reported in the literature for other Green's functions [6]; the radius of convergence of the Taylor series would exactly be zero. Although such difficulties can be circumvented, a practical implementation would become as difficult or more difficult than the Cauchy–Riemann equations. We have not pursued this matter further.

5 Summary and conclusions

We have presented a first analysis of the Cauchy–Riemann equations as applied to performing the inverse Wick rotation from Euclidean to Minkowski momenta. Given that their square is the elliptic Laplace equation, and that they are not of variational type [21], we do not have a trivial method to solve them to arbitrary accuracy. However, they provide an estimate of a function by analytical continuation as an initial value problem, that which relies only on the existence of a path on the complex plane that is free from singularities. While much mathematical literature exists [22] and more sophisticated solution methods have been reported, the very elementary methods presented here are sufficient to gain insight into the quark propagator mass function.

We obtain, after analytical continuation of the lattice QCD data, qualitatively backed up by a Dyson–Schwinger

calculation, and in agreement with recent studies, a pole of the quark propagator in Landau gauge QCD at or very near the real axis, with a mass of 305(25) MeV. We find no support for the sometimes conjectured pair of complex conjugate poles.

Acknowledgements The authors thank P. Bowman for his kind explanations and providing them with the quoted lattice data. Felipe Llanes-Estrada thanks the team at the Instituto Superior Tecnico de Lisboa for their hospitality during parts of this project. Mercedes Gimeno-Segovia thanks the "Excellence Scholarship Programme" of the Comunidad de Madrid for financial support. Work supported by grants FPA 2004-02602, 2005-02327, PR27/05-13955-BSCH (Spain) and Acción Integrada Hispano-Lusa HP2006-0018.

Appendix: Lorentz invariant discretizations in Minkowski space

Physical states provide representations of the rotation group. In lattice gauge theory, the symmetry of the grid reclassifies the states but at least offers some control over what signal may belong to what spin multiplet. This is because the lattice is invariant under a subgroup of the rotation group, typically tagged by a minimum angle $\theta = 90$ degrees. Likewise, the grid is invariant under a subset of the translation group characterized by the grid spacing a.

However, there is no equivalent parameter for finite grids in Minkowski space. A grid that is invariant under discrete Lorentz transformations has infinitely many points (and is therefore not tractable on a computer). We discuss this shortly as one more advantage of working in Euclidean space that may come into play when computing pdf's or reducing Green's functions in non-equal-time gauges such as the light-front gauge.

To see this, it is easiest to observe that Lorentz transformations map the light-cone to itself, acting as dilatations [19] within this manifold. To see it, it is simpler to work in $1+1$ dimensions, where the light-cone becomes the pair of lines

$$x = t; \qquad x = -t.$$

The action of the Lorentz boost becomes

$$\begin{pmatrix} t_1 \\ x_1 \end{pmatrix} = \begin{pmatrix} \gamma & \beta\gamma \\ \beta\gamma & \gamma \end{pmatrix} \begin{pmatrix} t_0 \\ x_0 = t_0 \end{pmatrix}, \tag{27}$$

hence

$$x_1 = t_1 = t_0(\gamma + \beta\gamma), \tag{28}$$

a dilatation of the parameter $\gamma(1+\beta)$. There is now an obvious way to construct a discretization of the light-cone that is invariant under Lorentz transformations of a fixed parameter γ. Simply pick an arbitrary point (t_0, x_0) and obtain

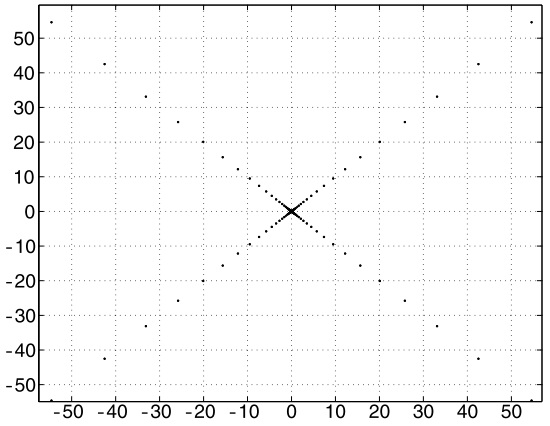

Fig. 13 A Lorentz transformation acts on the light-cone simply as a dilatation. Shown is a discretization invariant under a discrete Lorentz transformation, where each point on the plot is the Lorentz transformed point of its nearest neighbor towards the origin of coordinates. Note that this discrete transformation of the parameter $\Lambda \equiv \gamma(1+\beta)$ belongs to a subgroup of transformations with parameters $\Lambda^2, \ldots, \Lambda^n$, etc.

the sequence (t_1, x_1), $(t_2, x_2), \ldots$ obtained by successively applying (27) to it. The infinite sequence so obtained is such that every point j is the image of another point $j-1$ under a Lorentz transformation, except for $j = 0$. To generate this one, we furthermore need to also include in the discretization all points obtained by successively applying to (t_0, x_0) the inverse Lorentz transformation:

$$\begin{pmatrix} t_{-j} \\ x_{-j} \end{pmatrix} = \begin{pmatrix} \gamma & -\beta\gamma \\ -\beta\gamma & \gamma \end{pmatrix} \begin{pmatrix} t_{-j+1} \\ x_{-j+1} = t_{-j+1} \end{pmatrix}. \tag{29}$$

Thus, it appears that we have a simple discretization of the line $x = t$ that is invariant under discrete Lorentz transformations (dilatations in this line). It is, however, not invariant under translations, as the spacing between points $x_j - x_{j-1}$, $j > 0$, increases in proportion to their distance to the origin. Therefore, as is well known, one cannot construct a web that is simultaneously translation and Lorentz invariant, even under discrete Lorentz transformations.

This is different from the Euclidean space case, where the translationally-invariant Bravais lattices are also invariant under the discrete rotations of their corresponding crystallographic point group [18].

Moreover, grids that are invariant under a discrete Lorentz transformation have infinitely many points dense at the origin and infinity.

To construct a discretely Lorentz invariant lattice of the entire $1+1$ dimensional space, we just have to write down a discretization in which every point is the Lorentz transformed point of another one (and every Lorentz transformed point belongs to the lattice). Since Lorentz transformations leave the metric invariant, the hyperbolae $k^2 = (k^0)^2 - (\mathbf{k}^2) = m^2$ are invariant; that is, it is sufficient to construct a discretization of the hyperbola of (mass) parameter m. For

this, all one needs to do is to choose a point y_0 on the hyperbola and the discrete Lorentz transformation of parameter γ, and apply the Lorentz transformation and its inverse to generate the sequence of points

$$y_n = \Lambda(\gamma)^n y_0, \qquad y_{-n} = \Lambda(\gamma)^{-n} y_0.$$

Once this has been achieved, it is sufficient to pick up a set of hyperbolae to cover the entire space at wish and this completes the discretization.

To construct it, we start with a y_0 lattice in which there are points over both coordinate (x, t) axes. Then we obtain two families of hyperbolae with equations

$$\begin{aligned} H_1 &= \frac{x^2 - (ct)^2}{a_i^2} = 1, \\ H_2 &= \frac{(ct)^2 - x^2}{a_i^2} = 1, \end{aligned} \tag{30}$$

where $a_i = ia$ is the distance between their vertices (which will coincide with the chosen y_0) and the origin of the coordinates.

Note that the fact that a point and its Lorentz transformed point belong to H_1 or H_2 depends on whether the point lies within the forward or backward light-cones (hyperbolae of type H_2) or not (hyperbolae of type H_1). Note also that the successive Lorentz transformed images of a point under a discrete boost do not fill the hyperbola; they define a discrete lattice over it. All that remains to find is this subset of points.

A geometric way to map the discretization of one hyperbola to all others is to simply take straight lines through every point on the lattice covering the reference hyperbola and the origin.

This family of straight lines follow either of the rules (depending on the sign of the discrete Lorentz transformation employed in the construction):

$$\begin{aligned} (ct) &= \big(\tanh(i\varphi)\big)x, \\ (ct) &= \frac{1}{\tanh(i\varphi)}x, \end{aligned} \tag{31}$$

where φ is the discrete hyperbolic angle labeling the boost, and i the number of direct (positive i) or inverse (negative i) Lorentz transformations of the initial vertex.

Combining (30), and (31), we finally construct a Lorentz invariant lattice in $(1 + 1)$ dimensions of a chosen φ parameter at the intersections of the two families. The situation is plotted in Fig. 14.

Now, it is easy to observe that the hyperbolae contain all the images under direct and inverse Lorentz transformations of the vertex y_0, while the family of straight lines connect the points that correspond to the Λ^i image of each vertex across a family of hyperbolae.

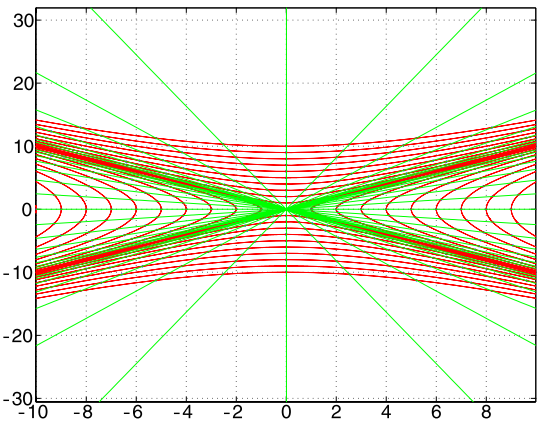

Fig. 14 The intersection points of a family of hyperbolae and a family of straight lines define a Lorentz invariant lattice of $1 + 1$ dimensional Minkowski space. The number of points in the lattice is infinite for any discrete set of boosts of parameter φ

References

1. D.M. O'Brien, Austral. J. Phys. **28**, 7 (1975)
2. M. Peskin, E. Schroeder, *An Introduction to Quantum Field Theory* (Westview, Boulder, 1995)
3. C. Itzykson, Zuber, *Quantum Field Theory Dover Publications* (Dover, New York, 2006)
4. P. Maris, C.D. Roberts, Int. J. Mod. Phys. E **12**, 297 (2003). arXiv:nucl-th/0301049
5. M. Creutz, Rev. Mod. Phys. **73**, 119 (2001). arXiv:hep-lat/0007032
6. R. Alkofer, W. Detmold, C.S. Fischer, P. Maris, Phys. Rev. D **70**, 014014 (2004). arXiv:hep-ph/0309077
7. R. Alkofer, W. Detmold, C.S. Fischer, P. Maris, AIP Conf. Proc. **756**, 272 (2005). arXiv:hep-ph/0411367
8. V. Sauli, J. Adam, P. Bicudo, Phys. Rev. D **75**, 087701 (2007). arXiv:hep-ph/0607196
9. V. Sauli, J. Adam, Phys. Rev. D **67**, 085007 (2003). arXiv:hep-ph/0111433
10. V. Sauli, J. Adam, Nucl. Phys. A **689**, 467 (2001). arXiv:hep-ph/0110298
11. K. Kusaka, A.G. Williams, Minkowski, Phys. Rev. D **51**, 7026 (1995). arXiv:hep-ph/9501262
12. J.M. Pawlowski, Ann. Phys. **322**, 2831 (2007). arXiv:hep-th/0512261
13. C.S. Fischer, J. Phys. G **32**, R253 (2006). arXiv:hep-ph/0605173
14. C. Bagnuls, C. Bervillier, Phys. Rep. **348**, 91 (2001). arXiv:hep-th/0002034
15. M.B. Parappilly, P.O. Bowman, U.M. Heller, D.B. Leinweber, A.G. Williams, J.B. Zhang, Phys. Rev. D **73**, 054504 (2006). arXiv:hep-lat/0511007
16. P. Bicudo, Phys. Rev. D **69**, 074003 (2004). arXiv:hep-ph/0312373
17. P.O. Bowman et al., Phys. Rev. D **76**, 094505 (2007). arXiv:hep-lat/0703022

18. A.L. Mackay, G.S. Pawley, Acta Cryst. **16**, 11–19 (1963). doi:10.1107/S0365110X63000037
19. H.C. Pauli, S.J. Brodsky, Phys. Rev. D **32**, 1993 (1985)
20. R. Alkofer, C.S. Fischer, F.J. Llanes-Estrada, K. Schwenzer, arXiv:0804.3042 [hep-ph]
21. R. Ferreiro Perez, J. Munoz Masque, Forum Math. **18**, 231 (2006)
22. A good compilation of articles can be found under http://math.fullerton.edu/mathews/c2003/CauchyRiemannBib/Links/CauchyRiemannBib_lnk_2.html